Femtosecond Laser Ablation Modeling of Tilted Microfeatures on Copper Surfaces

Pol Vanwersch[*1,2], Balasubramanian Nagarajan[1], Albert Van Bael[2], and Sylvie Castagne[1]

[1]*KU Leuven, Department of Mechanical Engineering and Flanders Make@KU Leuven - M&A, Leuven, Belgium*
[2]*KU Leuven, Department of Materials Engineering, Diepenbeek Campus, Belgium*
[*]*Corresponding author's e-mail: pol.vanwersch@kuleuven.be*

Femtosecond (fs) laser ablation produces precise microfeatures due to the laser-material interaction at timescales shorter than the electron-phonon coupling. In order to eliminate the extensive trial-and-error experimentation needed for for process optimization, modeling of fs laser ablation is often required. A pulse-based Two-Temperature Model (TTM) was developed in our previous work to predict the ablated groove geometry, and validated for low-corrosion tool steel. However, due to the complex laser-material interaction involved, it is necessary to validate the model for different materials, processing strategies and surface structures. This paper presents a comprehensive study on the prediction of fs laser-ablated inclined grooves on copper surfaces using the pulse-based TTM. In this work, the effect of inclination angle and process parameters such as scanning speed and laser fluence on the groove geometry were evaluated through simulation and experiments. The fabricated tilted grooves on copper surfaces were characterized using a cross-sectional optical microscopic analysis. The effectiveness of the calibrated TTM for predicting the geometry of the tilted grooves has been analysed. This paper underlines the potential of fs laser ablation for the manufacturing of highly precise tilted microfeatures and the suitability of the calibrated TTM for an accurate prediction of feature geometries.
DOI: 10.2961/jlmn.2023.03.2007
Keywords: femtosecond laser machining, modeling, ultrashort pulse, copper, inclined features

1. Introduction

Ultrashort pulse (~100s of femtoseconds) laser ablation is a highly precise process for the manufacturing of micro- and nanofeatures in a wide variety of materials [1]. However, the non-linear nature of the process, combined with the wide range of phenomena influencing the ablation makes it difficult to predict the feature geometry. Femtosecond laser ablation is commonly modelled by the Two-Temperature Model (TTM), where the spatial and temporal evolution of the electron and lattice temperatures are calculated [2]. The TTM has been widely used to understand femtosecond (fs) laser ablation phenomena [3], [4] but also to predict the ablation geometry [5]. In the latter case, a simplified version of the TTM, also called pulse-based TTM, can be used. In the pulse-based TTM, an estimation of the end state of the irradiated material following a fs pulse is made [2]. This approach, compared to the traditional approach of determining the state of the irradiated material at every time step during and following a pulse, is better suited for the prediction of features resulting of multiple pulses, thanks to its lower computational demands [6].

However, most of the current fs laser ablation modeling approach focusses on machining of flat surfaces despite an increasing demand to produce inclined microfeatures for different applications including heat transfer enhancement [7], cutting tools [8], 3D strain sensors [9] and optics [10]. Laser micromachining at an inclined angle has been experimentally studied in the literature [10]–[12] for different materials including stainless steel [13], silicon wafers [10], NiCr [9], elastomers [14] using nanosecond pulsed lasers [13], [14] or ultrashort pulsed lasers [9], [11], [15]. There have been attempts to model the fs laser ablation of inclined features [8], [9], [11], [12], [15] based on empirical equations and TTM. However, most of these modeling approaches are two-dimensional and do not take into account the full influence of the three-dimensional crater dimensions on the ablation process. The authors have previously developed a 3D fs laser ablation model based on pulse-based TTM to predict the shape and dimensions of the grooves and holes during laser micromachining [5], [16]. This pulse-based TTM, which includes correction factors for inclination- and orientation-dependent reflectivity, has been expanded in this work for the prediction of fs laser ablation of inclined features.

This paper assesses the performance of the pulse-based TTM for predicting the geometry of inclined grooves in copper after fs laser machining. The effects of laser pulse energy and the scanning speed on the inclined feature geometry at different inclination angles have been studied, by experiments and simulation.

2. Materials and method

2.1 Femtosecond laser micromachining

For this study, copper plates (99.9% purity) with a thickness of 1 mm and 0.1 µm surface roughness (R_a) were used as the substrate. Femtosecond laser machining of inclined grooves was conducted using a laser micromachining system with a fs laser source (CARBIDE, Light Con-

version Ltd.) with the following specifications: wavelength - 1030 nm, pulse duration - 250 fs, maximum average power - 20 W, maximum pulse energy - 400 µJ, maximum pulse repetition rate (PRR) - 1 MHz, focal length - 118 mm.

The spatial profile of the laser beam (Gaussian) was measured with a beam profiling camera (SP932U, Ophir Optronics Solutions Ltd.), and the beam focus radius – i.e. the radius at $1/e^2$ of the peak fluence – was measured to be 12 µm.

For determining the threshold fluence, single pulses with different fluences were irradiated on the flat copper plate. For every fluence level, four craters were created on the plate, and their radii were measured using a digital microscope (VHX-7000 with VH-ZST lens, Keyence, Japan). The common approach to determine the ablation threshold, developed by Liu [17], was used to correlate the crater dimensions and the threshold fluence.

Concerning the inclined grooves experiments, two plate holders with an inclination angle of 15° and 30° were 3D-printed with fused deposition modeling and placed on the linear stages of the fs laser machine. The polarization direction was chosen perpendicular to the scanning direction, as schematically depicted in Figure 1.

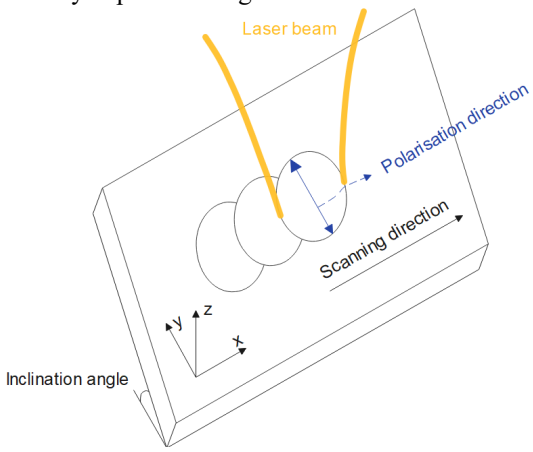

Fig. 1 Schematic of the laser scanning strategy. The axes represent the linear stages of the machine.

The scanning speed (250, 500, 750, 1000 mm/s), inclination angle (15°, 30°) and the pulse energy (9.5, 14.25, 19 µJ) were varied in this study whereas a constant PRR of 1 MHz was used for all the experiments. For each combination of scanning speed and pulse energy, three lines with a length of 10 mm were machined. Each line was repeated 20 times at the same location to increase the groove depth.

After laser machining, the lines were cross-sectioned in the middle (i.e., 5 mm from start and finish) using wire-electrical discharge machining before being hot-mounted, grinded and polished. The resulting cross-section profiles of the grooves were analyzed with the digital microscope.

2.2 Modeling of fs laser ablation of inclined features

The pulse-based TTM used in this work is based on a model developed for the prediction of microscopic fs laser-induced features in metals, which was validated for machining straight grooves and percussion drilling in steel using a fs laser [5], [16]. This is a 3D model, which calculates the ablation depth at every point after irradiating a pulse, based on the local fluence, the incubation factor and the local geometry. The equation for the ablation depth can be derived from the TTM [2] as follows:

$$z = max\{\delta \times ln(\frac{F_a}{F_{th}}), 0\} \quad (1)$$

where z is the ablation depth, δ is the optical penetration depth of electromagnetic radiation in the target material, which is also defined as the inverse of the absorption coefficient α. F_a is the absorbed laser fluence and F_{th} is the ablation threshold fluence, meaning that ablation will occur when $F_a > F_{th}$.

For multi-pulse irradiation, the threshold fluence and penetration depth have been reported to decrease with every pulse due to the heating up of the material. This can be represented by the following equations where S is the dimensionless incubation factor and N the number of pulses [18], [19].

$$F_{th}(N) = F_{th}(1) * N^{S-1} \quad (2)$$

$$\delta(N) = \delta(1) * N^{S-1} \quad (3)$$

For metals, S is typically equal to 0.8 [20]. However, for high numbers of pulses ($N > 20$), F_{th} and δ are constant and equal to $F_{th}(20)$ and $\delta(20)$, respectively [21].

In our previous work, a method for calculating the absorbed fluence was developed and validated for flat steel samples perpendicular to the laser beam [5]:

$$F_a(x,y) = F_c \times e^{-\left(\frac{2((x-x_c)^2+(y-y_c)^2)}{\omega_0^2}\right)} \times \frac{A_{proj}}{A_{real}} \times (1-R) \quad (4)$$

where F_c is the peak laser fluence, x_c and y_c are the coordinates of the pulse center, ω_0 is the beam focus radius at $1/e^2$ of the peak fluence, R is the reflectivity, and A_{proj}/A_{real} is the area correction factor. A_{real} is the actual surface area represented by mesh point (x, y), and A_{proj} is the projected surface area represented by the same point on a plane perpendicular to the propagation direction of the laser beam. The area correction factor allows the inclination of the local surface to be taken into account in a three-dimensional environment.

This approach relies on the inclination of the crater walls to define the local reflectivity and fluence distribution. As a result, predicting the ablation depth of inclined features can be done by starting from an inclined mesh. In other words, every mesh point is given an initial height z depending on the (x, y) position and the inclination angle. The area correction factor will then modify the local fluence accordingly.

For deep or inclined features, the beam divergence has a significant impact on the local fluence distribution. Therefore, ω_0 from equation (4) is replaced by the local beam radius $\omega_0(z)$, with z_{focus} the focus position and z_R the Rayleigh length:

$$\omega_0(z) = \omega_0 \times \sqrt{1 + \left(\frac{z - z_{focus}}{z_R}\right)^2} \quad (5)$$

For the simulations, the optical penetration depth for a single pulse $\delta(1)$ for copper was set to 44 nm, as reported by Byskov-Nielsen et al. (2010) [22]. The complex refrac-

tive index $\underline{n} = n + i\kappa$ was used to define the reflectivity of the material, with n the refractive index and κ the optical extinction coefficient. For 1030 nm wavelength, n and κ of copper are 0.34 and 6.77, respectively [23].

In order to predict inclined features, a mesh was created with a fixed orthogonal (x, y) grid, with variable z coordinates. The initial height of every mesh point was defined as $z(x, y) = y \cdot \tan(\theta)$ with θ the inclination angle. In this configuration, the ablation depth (i.e., the z-axis) was maintained along the beam propagation direction, similarly to the simulations at perpendicular incidence.

Thereafter, the simulation was performed similar to that of machining flat samples. During the simulations, the local ablation depth after every deposited laser pulse was calculated based on its distance to the pulse center, the focus depth, its local inclination and orientation, and the incubation factor. The simulation output was a three-dimensional surface mesh representing the predicted sample surface after ablation. The (x, y) resolution of the mesh was kept at 0.8 µm, which is in line with the convergence studies performed in the previous works [5]. A typical simulation result of an inclined groove at 15° is shown in Figure 2.

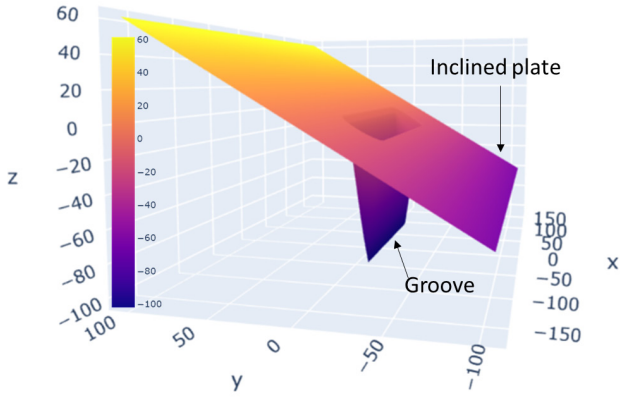

Fig. 2 Example of a simulated 3D inclined feature using the modified-TTM. The color bar indicates the local height. All units are µm.

The following analysis focuses on the shape and dimensions of the two-dimensional cross-sections of these grooves (read: y-z slice in the middle of the groove of Figure 2).

3. Results and discussion

3.1 Threshold fluence characterization

In order to determine the threshold fluence of copper at 1030 nm wavelength, pulses of varying fluences were deposited on a flat copper plate, perpendicular to the laser beam. The squares of the measured crater radii are plotted in function of the absorbed laser fluence in a semi-log plot in Figure 3.

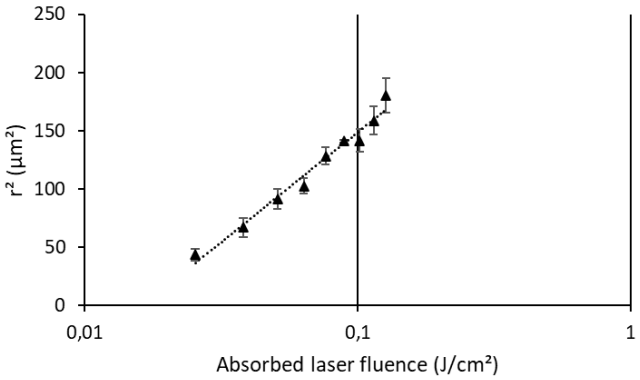

Fig. 3 Squared crater radius vs absorbed laser fluence for the determination of the threshold fluence according to Liu method. The error bars represent the standard deviation.

The fitted trendline crosses the x-axis at 0.016 J/cm², meaning that the fluence threshold at a single pulse, $F_{th}(1)$ is 0.016 J/cm², which was used in the simulation.

3.2 Femtosecond laser machining of inclined grooves

3.2.1 Groove morphology

Figure 4 shows the cross-sectional profiles of grooves fabricated at two inclination angles of 15° and 30° at different scanning speeds and a constant pulse energy of 19 µJ. It can be clearly seen that tapered grooves are inclined corresponding to the angles at which the samples were tilted (15° or 30°) during fs laser machining. A reduction in groove depth with increasing scanning speeds can also be noticed from Figure 4, due to the corresponding reduction in pulse overlap and hence the energy density. Another noteworthy phenomenon is the slight change in angle of the side of the groove, especially at 30° incidence. This could be due to multiple internal reflections on the side walls, which lead to increased ablation at the bottom of the groove, creating a thinner and deeper profile towards the bottom of the groove.

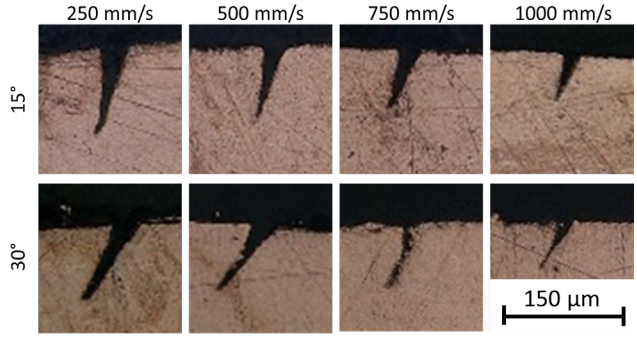

Fig. 4 Cross-sectional profile of fabricated inclined grooves at different scanning speeds [pulse energy = 19 µJ].

Figure 5 shows the corresponding cross-section profiles of the inclined grooves obtained by simulation. Firstly, it is obvious that the effect of scanning speed on the groove morphology from the simulation is similar to that of the experiments. Regarding the morphology of the simulated grooves such as depth, width and the inclination angles of the groove walls, they match the experimental results (Fig. 4) reasonably well at the lower scanning speeds (deeper grooves with sharp edges). However, there is an increasing discrepancy in the morphology at higher speeds.

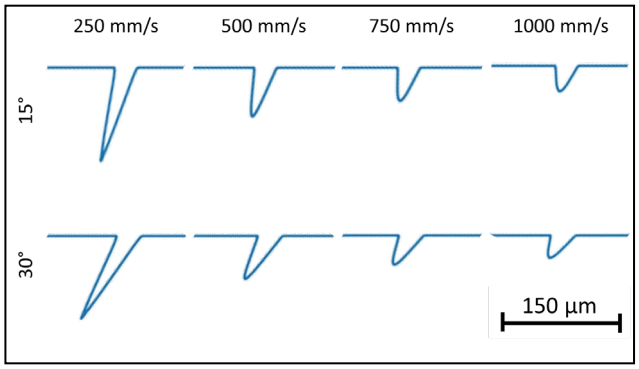

Fig. 5 Simulated cross-sectional profiles of inclined grooves at different scanning speeds [pulse energy = 19 µJ].

In order to clearly distinguish the inclined groove morphology between experiments and simulation, the results from two different conditions are overlayed in Figure 6. The grooves were made with 30° inclination angle, pulse energy of 19 µJ, and a scanning speed of 250 mm/s (Fig. 6a) and 1000 mm/s (Fig. 6b). It is clear that the simulation result at low scanning speed (250 mm/s) matches well with the experimental result in terms of groove profile, depth and width. However, Figure 6 (a) also shows that the simulated profile is slightly sharper towards the bottom of the groove than the experimental one. This can be attributed to the machining variations, as minor changes in the groove sharpness can also be noticed in Figure 4 for different scanning speeds. Concerning the grooves fabricated at a high scanning speed of 1000 mm/s (Fig. 6b), a larger difference can be noticed between simulation and experimental results. In this case, the simulated groove profile is similar to the experiment at the top of the groove, i.e., close to the surface. At about half of the groove depth, the experimental profile width is reduced to a narrow channel, which is not reflected in the simulation. As a result, the total groove depth is underestimated by the simulation, and also a large difference in the tip sharpness can be noticed.

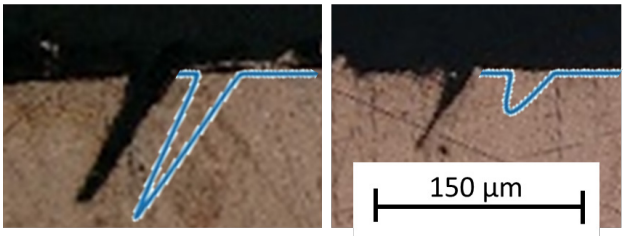

Fig. 6 Comparison of inclined groove morphology between experimental and simulation results at a) low (250 mm/s), and b) high (1000 mm/s) scanning speeds. The blue profile represents the cross-section of the simulated groove.

Figure 7 shows experimental and simulated cross-sections for varying pulse energies and inclination angles at 500 mm/s. Figure 7a highlights that a higher pulse energy results in deeper grooves. This trend is followed closely by the simulation results for both 15° and 30° configurations. Also, a slight increase in the width at the base of the groove with increasing pulse energy can be noticed for both experiments and simulations. Similar to the results observed in Figure 4 for higher scanning speeds, the simulated groove morphology is shallower and more-rounded, compared to the deeper grooves with sharp edges at the bottom.

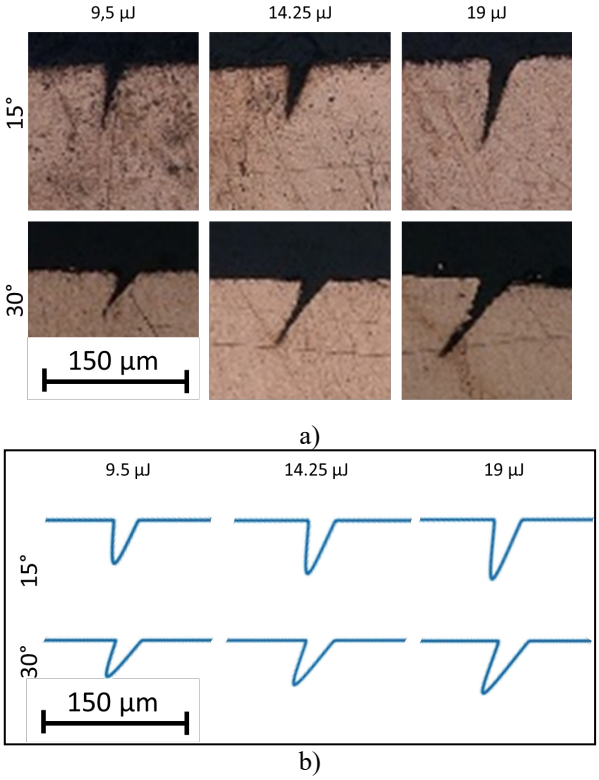

Fig. 7 Comparison of cross-sectional profiles of inclined grooves from a) experiments, and b) simulation, with varying inclination angle and pulse energy. The scanning speed is 500 mm/s.

3.2.2 Groove depth

Figure 8 compares the depth of the simulated and fabricated grooves, measured perpendicular to the top surface at varying scanning speeds for three pulse energies, 9.5 µJ, 14.25 µJ and 19 µJ.

It is clear from both the experimental and simulation results that a higher scanning speed and a lower pulse energy led to an obvious reduction in depth. At 250 mm/s, the simulated depth matches closely to that of the experiments, regardless of the pulse energy. However, the experimental depth decreased in a linear fashion with increasing scanning speed, while the simulated grooves tend to follow a non-linear trend. This caused a wider difference between simulations and experiments for scanning speeds above 250 mm/s. On an average, the simulated groove depths for scanning speeds greater than 250 mm/s are 36 ± 8% underestimated, in comparison to the experiments.

It can be noted from the experimental results that the higher inclination angle (30°) resulted in a shallower groove at a low pulse energy of 9.5 µJ compared to that of 15° angles. However, it is interesting to observe that the difference in depth between the inclination angles was greatly reduced at higher pulse energies (as seen in Fig. 8b and 8c) irrespective of the scanning speed, despite an increasing reflectivity of the laser beam at higher inclination angles. A possible explanation for this behavior could be the effect of beam scattering and reflection at the walls of the grooves during laser machining. Due to the higher an-

gle of the groove walls formed during the initial scanning passes at higher inclination angle, there could be prominent beam scattering and multiple internal reflection of the laser beam at the subsequent passes, which is beneficial in terms of increased energy density and groove depth.

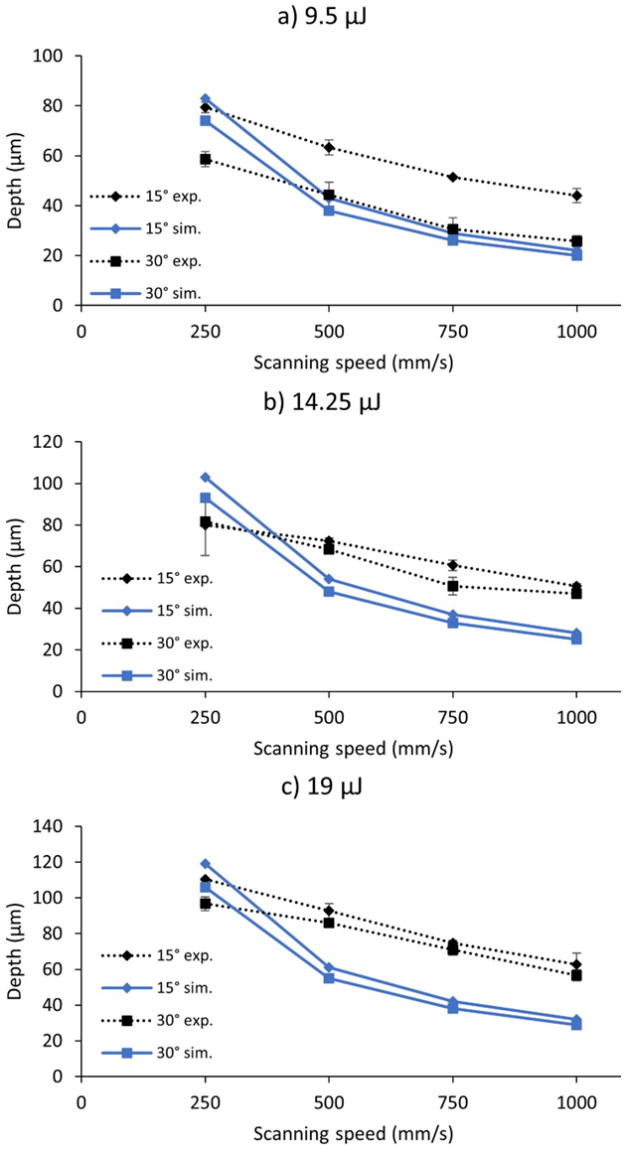

Fig. 8 Comparison of the experimental and simulated groove depth at 15° and 30° inclination for different scanning speeds and pulse energies. The error bars represent the standard deviation.

A similar behavior of increased light reflection from the inclined feature geometry was observed in the previous studies [11]. The correlation of this effect with the pulse energy indicates that there exists an optimal groove depth after which internal reflection effect becomes predominant. In the TTM, it is assumed that all the reflected energy is lost. However, in reality, some of the reflected energy contributes to ablation on the groove walls. This assumption could be attributed to the discrepancies between experimental and simulated groove morphology (Figs. 4 and 5) and depths (Fig. 8).

Furthermore, the incubation effect in the developed model might be different from the actual experimental conditions. Niso et al. [20] have experimentally found a decrease in the threshold fluence for a large number of pulses (N>20) in steel at large repetition rates (MHz regime) due to less efficient heat dissipation [20], and a similar phenomenon could occur in copper.

3.2.3 Groove width

Figure 9 depicts the width at the base of the inclined grooves (i.e., at the surface) for the simulated and experimental cross-sections for 9.5 µJ, 14.25 µJ and 19 µJ, respectively. The width of the inclined grooves was not widely influenced by the pulse energy. Concerning the influence of the scanning speed, a reduction in the fabricated groove width can be noticed for high speeds in Figs. 9b and 9c. However, the simulation results show a constant width across all scanning speeds, and a slight increase in width can be noticed for increasing pulse energy. Despite the minor variations, the simulated groove width matches the experimental results reasonably well, with an average error of 15 ± 8%.

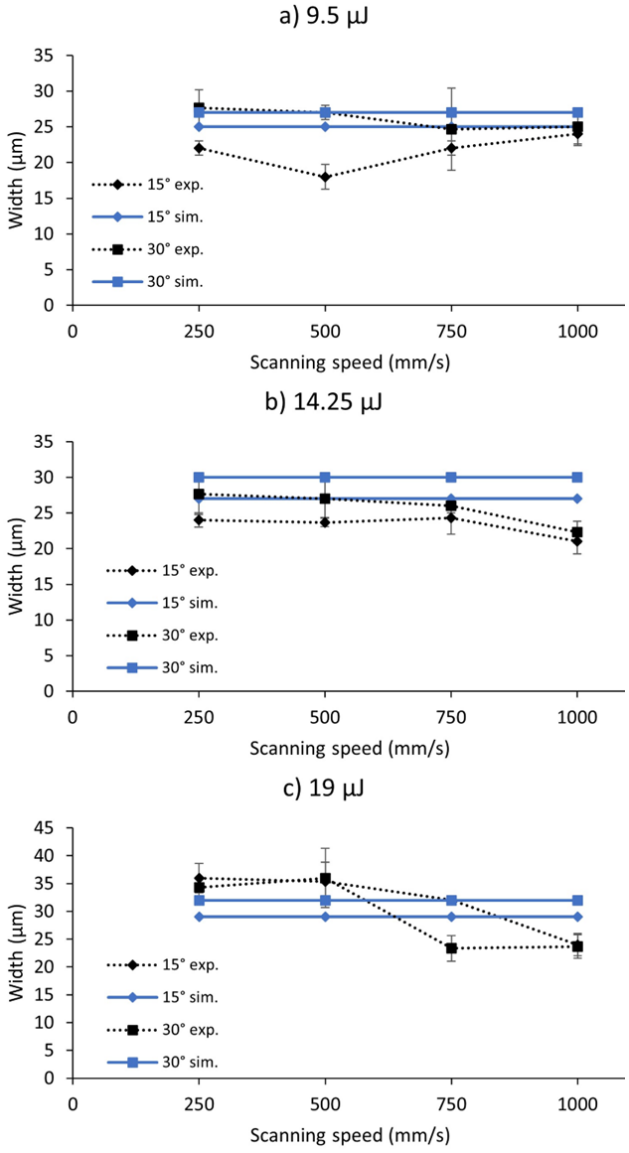

Fig. 9 Comparison of the experimental and simulated groove width at 15° and 30° inclination for different scanning speeds and pulse energies. The error bars represent the standard deviation.

4. Conclusion

In this work, an existing modeling approach based on pulse-based TTM was extended to predict the morphology of inclined grooves fabricated with femtosecond laser machining of copper with a linearly polarized beam. The results show that the overall trend of the simulated grooves matches well with the experiments for varying pulse energy and scanning speed. The shape and depth of the inclined grooves from the simulation correspond well to the experiments at low scanning speeds, but are underestimated at higher scanning speeds. However, the width of the simulated grooves match closely to the experimental results.

Acknowledgements

This research was supported by Internal Funds KU Leuven through the interdisciplinary network project IDN/20/011—MIRACLE, as well as the Fonds Wetenschappelijk Onderzoek (FWO)–Vlaanderen SB fellowship (1S31022N). The FWO Medium-Scale Research Infrastructure I001120N (FemtoFac) project is acknowledged for their financial support of the femtosecond laser equipment.

References

[1] K.-H. Leitz, B. Redlingshöfer, Y. Reg, A. Otto, and M. Schmidt: Phys. Procedia, 12, (2011) 230.
[2] B. N. Chichkov, C. Momma, S. Nolte, F. Alvensleben, and A. Tünnermann: Appl. Phys. A Mater. Sci. Process., 63, (1996) 109.
[3] Y.-H. Liu, C.-W. Cheng, and J.-K. Chen: J. Laser Micro Nanoengin., 15, (2020) 25.
[4] L. L. Dasallas and W. O. Garcia: Mater. Res. Express, 5, (2018) 016518.
[5] P. Vanwersch, S. Schildermans, B. Nagarajan, A. Van Bael, and S. Castagne: Lasers Manuf. Mater. Process., 9, (2022) 515.
[6] E. Audouard and E. Mottay: Front. Ultrafast Opt. Biomed. Sci. Ind. Appl. XVI, 9740, (2016) 974016.
[7] G. Liang and I. Mudawar: Int. J. Heat Mass Transf., 128, (2019) 892.
[8] P. Boerner, M. Hajri, T. Wahl, J. Weixler, and K. Wegener: J. Appl. Phys., 125, (2019) 234902.
[9] L. Overmeyer, J. F. Duesing, O. Suttmann, and U. Stute: CIRP Ann., 61, (2012) 215.
[10] X. H. Wang, P. T. Lai, and H. W. Choi: J. Vac. Sci. Technol. B Microelectron. Nanom. Struct. Process. Meas. Phenom., 27, (2009) 1048.
[11] D. G. K. Aboud, A. Gruner, and A.-M. Kietzig: Appl. Phys. A, 128, (2022) 1057.
[12] M. Hajri, P. Börner, and K. Wegener: Procedia CIRP, 74, (2018) 709.
[13] S. Pattanayak, S. Panda, and D. Dhupal: J. Manuf. Process., 52, (2020) 220.
[14] G. Kravanja, I. A. Belyaeva, L. Hribar, I. Drevenšek-Olenik, M. Shamonin, and M. Jezeršek: Adv. Mater. Technol., 7, (2022) 2101045.
[15] A. Michalek et al.: Appl. Surf. Sci. Adv., 2, (2020) 100036.
[16] P. Vanwersch, B. Nagarajan, A. Van Bael, and S. Castagne: Micromachines, 14, (2023) 593.
[17] J. M. Liu: Opt. Lett., 7, (1982) 196.
[18] Y. Jee, M. F. Becker, and R. M. Walser: J. Opt. Soc. Am. B, 5, (1988) 648.
[19] B. Neuenschwander, B. Jaeggi, M. Schmid, A. Dommann, A. Neels, T. Bandi, and G. Hennig: Proc. SPIE, 8607, (2013) 86070D.
[20] F. Di Niso, C. Gaudiuso, T. Sibillano, F. P. Mezzapesa, A. Ancona, and P. M. Lugarà: Opt. Express, 22, (2014) 12200.
[21] K. M. Ahmmed, C. Grambow, and A.-M. Kietzig: Micromachines, 5, (2014) 1219.
[22] J. Byskov-Nielsen, J. M. Savolainen, M. S. Christensen, and P. Balling: Appl. Phys. A Mater. Sci. Process., 101, (2010) 97.
[23] P. B. Johnson and R. W. Christy: Phys. Rev. B, 6, (1972) 4370.

(Received: July 6, 2023, Accepted: October 12, 2023)